The Representation of the Visual Field in the Lateral Geniculate Nucleus of *Macaca mulatta* [1]

JOSEPH G. MALPELI [2] AND FRANK H. BAKER
Departments of Ophthalmology and Physiology, The Johns Hopkins University School of Medicine, Baltimore, Maryland 21205

ABSTRACT Microelectrode recording techniques were used to investigate the projection of the visual field into the lateral geniculate nucleus (LGN) of *Macaca mulatta*. The data were used to construct charts plotting visual direction, designated in terms of azimuth and elevation, onto sections of the nucleus cut in coronal, sagittal and horizontal Horsley-Clarke planes. The projection of the horizontal meridian divides the LGN along its plane of symmetry into a medial-superior half having negative elevations and a lateral-inferior half having positive elevations. Elevations become more positive or negative with distance from this plane. Azimuths closest to the vertical meridian are located posteriorly, while the most peripheral azimuths are found at the anterior pole. Two families of surfaces representing visual directions of constant azimuth and elevation are described. Visual field zones of increasing eccentricity are represented serially along the posterior-anterior axis of the LGN, with the foveal area restricted to the posterior pole and the monocular crescent projecting to the anterior pole. The mapping is completely continuous across the horizontal meridian. The edges of the stacked cell laminae exposed around the periphery of the LGN form an oval band which receives the projection of the perimeter of the contralateral hemifield. The vertical meridian is represented by the posterior two-thirds of this band, while the periphery of the hemifield projects to the anterior third.

The central visual field out to the optic disc is represented by six cell layers, while the rest of the binocular field projects to four layers only (2 parvocellular and 2 magnocellular). The monocular crescent is represented by one parvocellular and one magnocellular layer. Features associated with the projection column of the optic disc are integrated into the transition from six to four layers. Details of the receptive field topography in the vicinity of the optic disc discontinuities indicate that these gaps are produced by intralaminar mechanisms.

The magnification factor (mm^3/steradian) increases monotonically from peripheral visual fields to the foveal center, varying over a range of three decades. This range is intermediate between those derived from data reported in the literature for the retina and the striate cortex. The ratio of LGN magnifications at any two angular eccentricities is a power function, with an exponent of 1.34, of the corresponding ratio of retinal ganglion cell densities. Similarly, the ratio of cortical magnifications (mm^2/steradian) at any two eccentricites is a power function, with an exponent of 1.35, of the corresponding ratio of LGN magnifications.

In primates, as in other mammals, the visual field is represented in the lateral geniculate nucleus (LGN) in an orderly topographical fashion. The general outlines of the projection of the retina to the primate LGN were deduced from experiments utilizing retinal lesions (Brouwer and Zeeman, '26; Clark and Penman, '34; Polyak, '57). It was not possible, however, to resolve the finer aspects of the projection with the anatomical techniques available. Recently, electrophysiological data have been obtained which differ somewhat from the results of lesion experiments. Kaas et al. ('72) corrected errors in the scale of representation of the central visual fields and in the

[1] Send reprint requests to: Dr. Frank H. Baker, Dept. of Ophthalmology, The Johns Hopkins University School of Medicine, Rm. 355 Woods Research Bldg., 601 N. Broadway, Baltimore, Md. 21205.
[2] Present address: Department of Psychology, Building E10–018, Massachusetts Institute of Technology, Cambridge, Massachusetts 02139.

location of peripheral visual fields in the LGN. A map of the outermost lamina of the LGN published by Whitteridge ('73) differs significantly from the arrangement expected from the earlier lesion work.

We have undertaken an investigation of the projection of the visual field into the LGN of *Macaca mulatta* in order to produce a map of sufficient resolution and completeness to make possible a fuller understanding of the topography of the representation. We used microelectrode recording as a method for mapping receptive field locations within the LGN. Since we decided that the complexity and morphological variability of the macaque LGN would make it difficult to assemble an atlas from partial mappings of many different nuclei, we did a complete charting of a single LGN, expecting that the general features would be consistent from animal to animal. Data from less completely mapped nuclei verified this assumption. The charts thus produced enabled us to determine the number of cell laminae devoted to different areas of the visual field and to formulate a theory of the origin of the cell discontinuities associated with the optic disc. We also calculated magnification factors for the LGN at eccentricities from 0° to 60° and compared these to the data obtained by other workers for the retina (Rolls and Cowey, '70) and the striate cortex (Daniel and Whitteridge, '61).

METHODS AND MATERIALS

A. *Animal preparation and electrophysiological recording techniques*

Our method of acute microelectrode recording was basically that described by Poggio et al. ('69), in which the head was held by a hydraulically sealed cylinder stereotaxically implanted on the skull. A glass guard tube was stereotaxically driven through the chamber into the brain to a point 5 to 8 mm above the left LGN. Glass-insulated platinum-iridium microelectrodes were then passed through the guard tube and into the LGN with a hydraulic drive. Neural signals were amplified and monitored with an oscilloscope and loudspeaker.

The animals were paralyzed with a continuous intravenous infusion of gallamine triethiodide (15 mg/kg/hr). Accommodation was paralyzed and the pupils were dilated with atropine sulfate. Contact lenses kept the corneas moist and brought the eyes to focus at about 60 cm, as determined by slit retinoscopy. Periodically, the contact lenses were removed and the eyes irrigated with warm saline for several minutes.

B. *Receptive field localization*

Bishop et al. ('62) have discussed the relative advantages of several coordinate systems which can be used for recording direction in visual space. We adopted the one used by Bishop et al. ('62) and Sanderson ('71) in studies of the cat LGN.

In this coordinate system (fig. 1), visual directions relative to the primary visual direction (foveal ray) are assigned two angles: azimuth (A) and elevation (E). These angles lie in two mutually perpendicular planes: one containing the projection of the horizontal meridian and one dropped through the ray of visual direction. Azimuth is defined as the angle between the intersection of these two planes and the ray representing the foveal projection. Elevation is defined as the angle between the intersection of the planes and the ray representing visual direction. Thus the coordinates of the center of the fovea are azimuth = 0, elevation = 0. Elevations above and azimuths to the right of the origin are taken to be positive. The main advantage of this

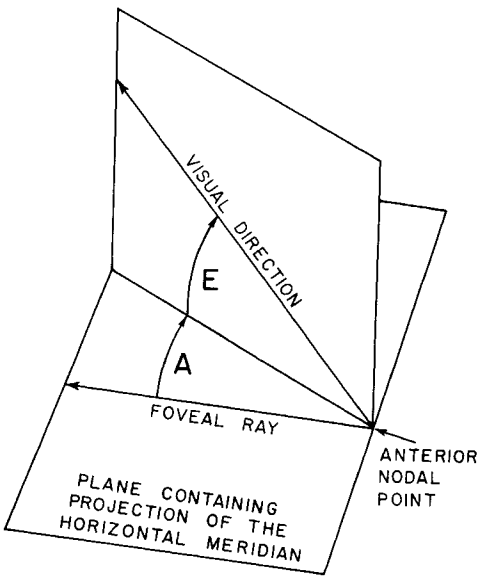

Fig. 1 Diagram showing how visual direction is defined in our coordinate system by azimuth (A) and elevation (E). The two planes are mutually perpendicular.

coordinate system over its alternatives is that in the central visual fields it is rectilinear and both coordinates are equivalent in terms of actual distances on the retina.

A hand-held projector was used to locate receptive fields on a rear projection perimeter screen of radius 57.3 cm constructed so as to allow direct reading of azimuth and elevation. Readings were taken to the nearest tenth of a degree. The pivot point of the screen could be shifted readily to lie under either eye, thus providing compensation for interpupillary distance.

The foveas were located on the screen by a device which positioned a small mirror in front of the cornea from which a beam of light was reflected onto the fundus. The beam contained a cross-hair pattern which could be brought to focus on the retina, viewed directly with an ophthalmoscope, and positioned on the center of the foveal pit with micrometer adjustments. A calibration procedure related the micrometer readings to positions on the perimeter screen.

C. *Histology*

Positions along electrode tracks were marked with lesions made by passing direct current (2–10 microamp for 2–10 sec) through the microelectrode tip. At the end of the experiment steel needles were driven into the brain around the LGN to aid in shrinkage calculations. The monkey then was perfused with Krebs solution followed by 10% buffered formalin. The calvarium was removed and the head immersed in 10% buffered formalin for one to two days. The head was remounted in a stereotaxic apparatus and sharpened steel rods were driven into the brain to guide cuts for removing the LGN in a block cut in Horsley-Clarke planes. After fixation was completed in 10% formalin, the block was washed, dehydrated, and embedded in celloidin. The left (experimental) LGN's were cut coronally in 25-micron serial sections, mounted, and stained with thionine. The right LGN's were cut either sagittally or horizontally.

RESULTS

A. *Data collection*

The methods described above were used to map the left LGN's of three monkeys. Generally, microelectrode penetrations were placed in rows along coronal planes and passed completely through the nucleus. The number of penetrations intersecting LGN's 1, 2, and 3 were 17, 18, and 33, respectively. On the basis of the number and distribution of data points (fig. 2), LGN 3 was chosen for a complete visual field reconstruction.

The electrodes used recorded at most a weak unresolved background from axons in the fiber capsule surrounding the LGN and in the optic tract. Entry into and exit from the LGN were well defined, as were the relatively quiet regions between layers. The great majority of isolated neurons had action potentials with the duration, polarity, waveform, and amplitude modulation characteristic of cell bodies rather than axons (Bishop et al., '62). Single isolated neurons and multineuron records were generally used for receptive field localization, although unresolved background activity was occasionally accepted. The receptive field coordinates assigned to neural activity at a given point in a penetration were the coordinates of the center of the receptive field area of that activity. This area was delimited with small spots of light, using an audio monitor to evaluate the neural re-

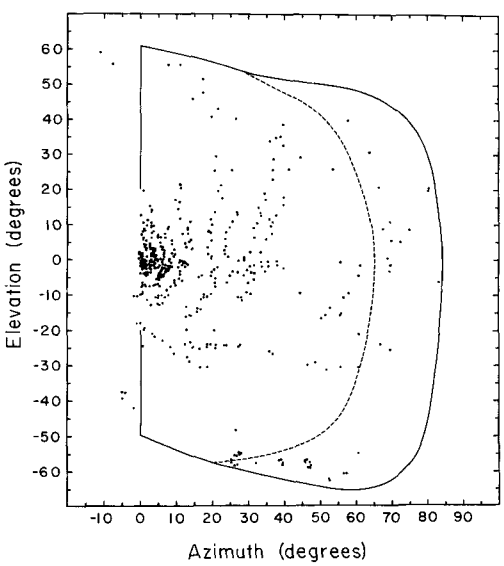

Fig. 2 Receptive field locations of data points in LGN 3. Not all points are shown because of crowding. The solid line delineates the visual field area which is included in our reconstructions on Horsley-Clarke planes (figs. 5a,b,c). The entire visual hemifield is undoubtedly larger. The broken line indicates our estimate of the boundary between binocular and monocular fields.

sponse. The receptive fields of both single neurons and multineuron records were almost always small and well defined, and we believe that relative to the scale of our reconstructions, no significant errors were introduced by inaccurate delineation of the receptive field area.

Data consisted of the electrode depth, receptive field coordinates, ocular dominance, and type of record (isolated neuron, multineuron record, or background), at the location being investigated. These parameters were continuously monitored and data were recorded when a significant shift in receptive field location was observed, or when the electrode had been advanced 150 to 200 microns from the previous data point, or upon entry into or exit from a cell layer. Occasionally, neural activity was recorded from what were taken to be interlayer regions.

In order to minimize vertical stereotaxic errors, microelectrodes were changed as seldom as possible. For LGN 3, a single microelectrode was used for the entire experiment. Evaporation of fluid from the hydraulic microelectrode-drive (David Kopf Instruments, Model 12075) required the vertical stereotaxic coordinates of the microelectrode tip to be corrected for an upward drift of 3.5 microns/hr.

Foveal position was determined at the beginning of each recording session and at the end of each penetration. Shifts as large as 0.5° were often seen, especially in the horizontal direction. The magnitude of these shifts varied from animal to animal. In monkey 3, they were generally less than 0.1° over the course of a single penetration.

B. *Morphological reconstructions*

The electrode tracks of all but two penetrations in the three LGN's were identified and the paths of the electrodes through the LGN determined. The last penetrations in LGN's 1 and 3 were made immediately before the animal was killed, and there was not enough time for gliosis to occur. The data from these two penetrations were still used, however, with the stereotaxic coordinates of the penetrations relied upon for determining the paths of the microelectrode tips.

Microelectrodes were carefully selected for straightness, and there was no evidence of significant deviations of their paths through the brain. Electrode tracks were generally curved, but the uniform progression of direction of curvature across a coronal section indicated that the curvature was a result of differential shrinkage of the tissue blocks. This was further supported by the tracks left by the steel needles driven around the LGN at the conclusion of each experiment. Although these needles were much too stiff to have been deviated, their tracks in the tissue sections showed the same curvature as the adjacent electrode tracks.

Tracings were made of the coronal sections containing rows of microelectrode tracks. Shrinkage was taken into account by enlarging the traced sections to match the outlines determined by the electrophysiological mapping. Differential shrinkage caused a distortion of shape as well as size, and this distortion was maximum near the invagination of the ventral surface of the nucleus known as the "hylum." This was compensated for by reshaping the traced sections slightly to obtain a better correspondence to the electrophysiologically determined outlines. The original tracings and the reshaped outlines are shown in figure 3.

The coronal tracings of LGN 3, corrected for shrinkage, in turn were used to construct sagittal and horizontal series of outlines. These may be seen in figure 5 and in an abbreviated version in figure 12. A solid model of LGN 3 was also reconstructed from the coronal tracings, and some views of this are shown in figures 6a and 6c. (Other features of these figures are discussed later.)

On the basis of our experience (11 serially sectioned LGN's), LGN 3 is about average in size, shape, and orientation for this species. It is the left LGN of a 4.3 kg female macaque. The posterior pole is higher and more lateral than the anterior pole: the inclination of the major axis is about 35° with respect to the horizontal and 15° with respect to a sagittal plane. It also tilts laterally, its plane of symmetry forming an angle of approximately 40° with the sagittal. Its length along the major axis (a line lying in the plane of symmetry and connecting the anterior and posterior poles) is 8.5 mm. The volume of the nucleus, including the interlayer regions, is approximately 77 mm^3. The protuberance seen on the dor-

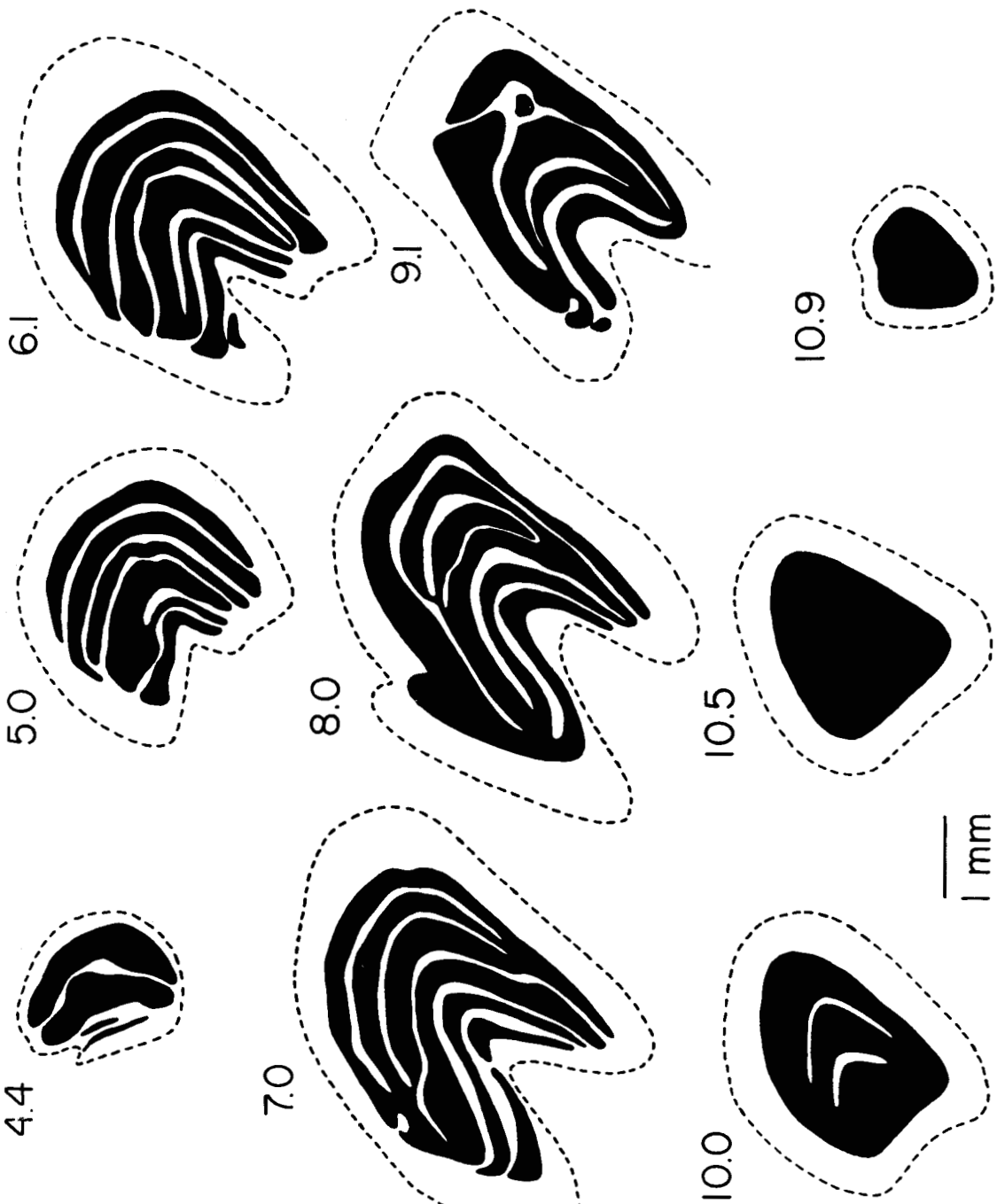

Fig. 3 Tracings of coronal sections of LGN 3 at the Horsley-Clarke anterior levels indicated. These are levels where microelectrode penetrations were made. The dotted outlines show the contours of the nucleus after compensation for shrinkage distortion. The lamination pattern near the anterior pole is difficult to follow in coronal sections since the layers are almost tangent to the coronal plane.

sal-medial aspect of the LGN (figs. 6, 5a, A = 8.0 mm) is actually partially detached from the main body of the nucleus. A similar feature was found in the right LGN of this animal. Islands of cells detached from the main body of the LGN are common.

The ventral projections of the nucleus which surround the hylum will be referred to as the medial and lateral wings of the LGN. The medial wing extends farthest from the main body of the LGN at a point about midway between the posterior and anterior pole. The lateral wing, which does not protrude as far as the medial wing, reaches its greatest development considerably closer to the anterior pole.

Different LGN's show considerable variations in orientation, size, shape, and location with respect to Horsley-Clarke coordinates. Clearly, differences in orientation alone will result in apparent differences in size and shape when the LGN is viewed in cut sections.

C. *Reconstruction of isoazimuth and isoelevation surfaces*

It has long been recognized that a small region of the visual field projects to a column of cells which extends from the hylum to the dorsal surface of the LGN (Clark, '41a; Clark and Penman, '34). Thus a point in the visual field projects to the LGN as a line, called a "projection line" by Bishop et al. ('62). Anatomical and electrophysiological experiments have shown that the projection of the retina into the monkey LGN is topographically organized. If this holds true at the finest levels of organization, then the family of projection lines representing the locus of points forming a line on the retina determines a surface which passes through the LGN from the most ventral to the most dorsal layers. Just as a point in the visual field can be defined by the intersection of an azimuth and an elevation line in the coordinate system used in this report, so a projection line in the LGN can be defined by the intersection of an isoazimuth and an isoelevation surface. The projection of the visual field into the LGN can be represented by two intersecting families of surfaces: one for azimuth and one for elevation.

These concepts have been elegantly developed by Bishop et al. ('62), who showed that visual directions of constant elevation or azimuth are projected into the LGN of the cat as surfaces that are approximately planar. (See Sanderson, '71 for a detailed mapping of the cat LGN.)

The morphological complexity of the monkey LGN made it seem likely that its isoazimuth and isoelevation surfaces would be complex, making the fitting of a smooth family of surfaces to data points distributed throughout the volume of the LGN a difficult task. We simplified the data reduction by fitting isoazimuth and isoelevation curves (the intersections of isoazimuth and isoelevation surfaces with planes cutting through the LGN) to the data points on Horsley-Clarke planes. To make efficient use of all data points and to insure that these curves adequately represent the contours of the surfaces generating them, it was necessary to work simultaneously with coronal, sagittal, and horizontal planes. What follows is a detailed description of the manner in which we handled the data from LGN 3.

Before using the visual direction data for visual field reconstructions, it was necessary to consider eye rotation about the optic axis. To determine the degree of rotation by viewing the fundus of the paralyzed animal required that the fovea and a landmark on a known meridian be projected to the perimeter screen. The obvious landmark is the optic disc, but we did not know its visual field coordinates in *Macaca mulatta*. In monkey 3, both optic disc centers projected to the same elevation with respect to the corresponding fovea. Therefore, if the two eyes were rotated about the optic axis, they were rotated to the same extent, but in opposite directions. To determine the degree of rotation and correct the data for it we made two graphs for each penetration: electrode depth versus azimuth and electrode depth versus elevation. Any given rotation of the eyes with respect to one another should have caused abrupt shifts in these curves of predictable direction and magnitude associated with shifts of ocular dominance. However, no significant and consistent shifts were seen, indicating that there was no rotation for which to correct (fig. 4 for an example). Having taken rotation about the optic axis into account, we could now determine the true visual field position of the optic disc, and it turned out to be centered on the horizontal meridian

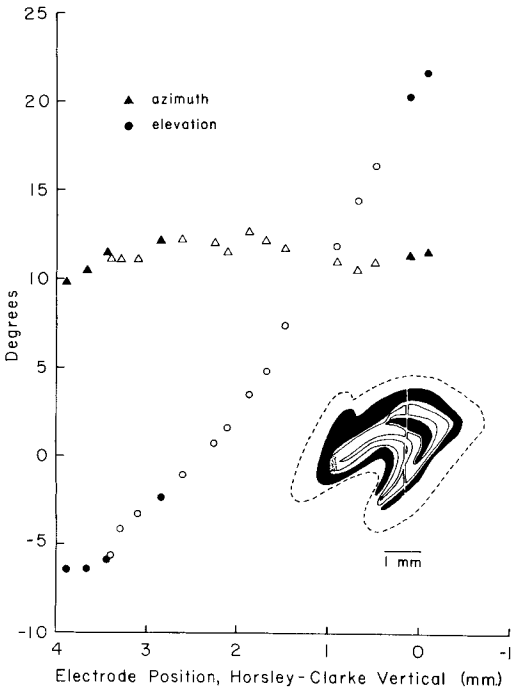

Fig. 4 Results of a typical microelectrode penetration through the central portion of LGN 3. Filled in symbols are for locations activated by the contralateral eye. The path of the microelectrode is indicated on the tracing of the coronal section (Horsley-Clarke anterior = 8.0 mm.). The dotted line shows the outline of the nucleus after compensation for shrinkage distortion. There were five other penetrations at this coronal level. Contralateral-eye layers are blackened in. The strippled area was not clearly divided by an interlaminar zone, so no designations are made as to eye dominance.

approximately 17 degrees from the center of the fovea.

Azimuths and elevations (referred to here as "data points") were plotted along electrode tracks in the coronal and sagittal series of drawings of LGN 3 and beside intersections of electrode penetrations with the horizontal series of outlines. Since the projection of the visual field into the LGN is continuous across the laminae of the nucleus, the lamination pattern and ocular dominance were ignored in these constructions. Isoelevation curves were fitted to the elevation data on the coronal series, producing a tentative family of curves on each coronal plane. Curve fitting was guided by the assumption that nearby isoelevation lines would tend to run parallel to each other and that linear interpolations over short distances were valid. Points on these curves at the intersections of the coronal and sagittal series of planes were transferred to the sagittal series, where along with the data points they were used to construct an isoelevation family of curves on the sagittal series. In constructing these curves much more weight was given to data points than to the points derived from the tentative curves on the coronal series, so that the curves on the sagittal and coronal series generally did not match at this stage of the data reduction. Points on the sagittal series of curves at the intersections of the coronal and sagittal series of planes were then transferred back to the coronal series. The original coronal family of curves was re-evaluated against these points and the data points, and adjusted where necessary. This process of successive approximations, in which progressively finer adjustments were made while switching back and forth between the coronal and sagittal series, continued until the same family of isoelevation curves fit the data in both coronal and sagittal planes. Then the curves were transferred to the horizontal series and the process repeated for all three Horsley-Clarke planes until all data points in all three series were well matched by reasonably smooth progression of curves. The same method was used to reconstruct the isoazimuth family of curves on the three series of Horsley-Clarke planes.

The results derived from these procedures are shown in figures 5a,b,c. These charts served as the basis for all other graphic displays of the representation of visual fields in the LGN presented in this report.

Data from monkeys 1 and 2 were checked against these results. Figure 7 is a projection of the dorsal surface of LGN 3 on which lines of constant azimuth and elevation are drawn. The anterior and lateral Horsley-Clarke coordinates of the point on figure 7 having the same visual field coordinates as the first point of contact (touchdown point) of a given microelectrode penetration through LGN 1 or 2 were obtained. Then the progressions of azimuths and elevations in LGN 3 along a vertical line with these same anterior-lateral coordinates were determined from figure 5c, and compared to the curves of azimuth versus electrode depth, and elevation versus electrode depth,

for the penetration in LGN 1 or 2 being examined. A good correspondence, both in trend and magnitude, was found. The metric on the dorsal surface of the LGN was also checked against LGN's 1 and 2. Differences in visual direction between touchdown points of pairs of penetrations in LGN's 1 or 2 were compared with the differences predicted from figure 7. Again, a close correspondence was found. Our successful use of these charts as a guide for the placement of microelectrodes in specific receptive field locations of the LGN has strengthened our belief that their main features are consistently present in the macaque LGN.

Our data are presented in the format of an atlas. As we have already noted, however, the position of the LGN with respect to the Horsley-Clarke origin is variable, so the Horsley-Clarke coordinates given apply to LGN 3 alone. For the experimentalist concerned with locating a specific region of the LGN, a reference microelectrode-penetration into the nucleus must first be made. Figures 5 and 7 can then be used to guide the electrode in successive penetrations to the region desired. It is often useful to continue this first reference penetration through the LGN, noting the progression of azimuths and elevations, in order to judge the orientation of the nucleus relative to LGN 3.

D. *General features of the mapping*

An inspection of figures 5, 6, and 7 shows that the isoelevation surfaces run in the anterior-posterior axis of the LGN, fanning out from the hylum. The zero elevation surface occupies a central position, forming a surface of symmetry about which the upper and lower visual fields project. Positive elevation surfaces are found lateral to this surface and negative surfaces are medial. Extremes of elevation are located in the tips of the medial and lateral wings of the LGN. A sample elevation surface ($-8°$) is shown in its entirety in figure 6b.

The isoazimuth surfaces are more complex. Generally, they are cupped so as to appear concave when viewed from a point anterior to the LGN. An example (20°) is shown in figure 6d. The lowest azimuths are in posterior regions of the nucleus and the highest are anterior (fig. 5b). The surfaces lie roughly parallel to the coronal plane in the posterior pole, but gradually turn to lie more in the sagittal plane in the anterior pole. In doing so they become asymetrically placed with respect to the main axis of the LGN, and the highest azimuths are found on the medial side of the anterior pole. At this location, the extreme isoazimuth surfaces intersect both positive and negative isoelevation surfaces to represent the extreme peripheral receptive fields (fig. 5a, A = 10.0, 10.5, and 10.9; fig. 6a,c). Since all isoazimuth surfaces cross the 0° elevation surface, upper and lower peripheral visual fields are not physically separated by the central fields and hylum as Polyak ('57) believed. Rather, the mapping is topographically continuous throughout the entire visual field. Low azimuths, while having their greatest representation in the posterior pole, also extend forward along the outer rims of the medial and lateral wings where they intersect extremes of elevation. As can be seen in figures 6a,b, the 1° azimuth surface extends

Fig. 5 *Key to isoazimuth and isoelevation charts.* The coronal (a), sagittal (b), and horizontal (c) series are presented in standard Horsley-Clarke coordinates. The scales are in millimeters, and show the actual coordinates for LGN 3. The bold-face characters A, L, and H refer respectively to distances anterior to, to the left of, and above the coronal, sagittal, and horizontal planes passing through the Horsley-Clarke origin. The coronal planes chosen are those in which rows of electrode penetrations were made. The sagittal planes are spaced 1 mm apart in the lateral portion of the LGN and 0.5 mm apart in the medial portion where the isoazimuth and isoelevation curves are shifting rapidly. Following the progressive shifts in the curves on the horizontal series requires 0.5 mm spacing of the horizontal planes in several areas, so the entire horizontal series is presented at a spacing of 0.5 mm. Isoazimuth curves are represented with broken lines and isoelevation curves with solid lines. Generally, the same progressions of azimuths and elevations are represented, so that only a few curves are labeled. The azimuths represented are: 1, 2, 4, 8, 12, 16, 20, 30, 40, 50, 60, 70, and 80 degrees. For elevations, the progression is: 0, ±2, ±4, ±8, ±12, ±16, ±20, ±30, ±40, ±50, ±60 degrees. These azimuths and elevations will be referred to as the "standard progression." In some areas the curves are too closely spaced to be fully represented and certain curves of the standard progression are deleted. In these cases every curve in this portion of the progression is labelled. In some of the coronal and horizontal sections the 1° elevation line is added and so labeled. Where curves are not labeled, the standard progression is assumed. A number in parenthesis refers to a single data point rather than a line. No isoazimuth lines are shown in *a* (A = 4.4) because all azimuths in this coronal plane are less than 1° from the vertical meridian.

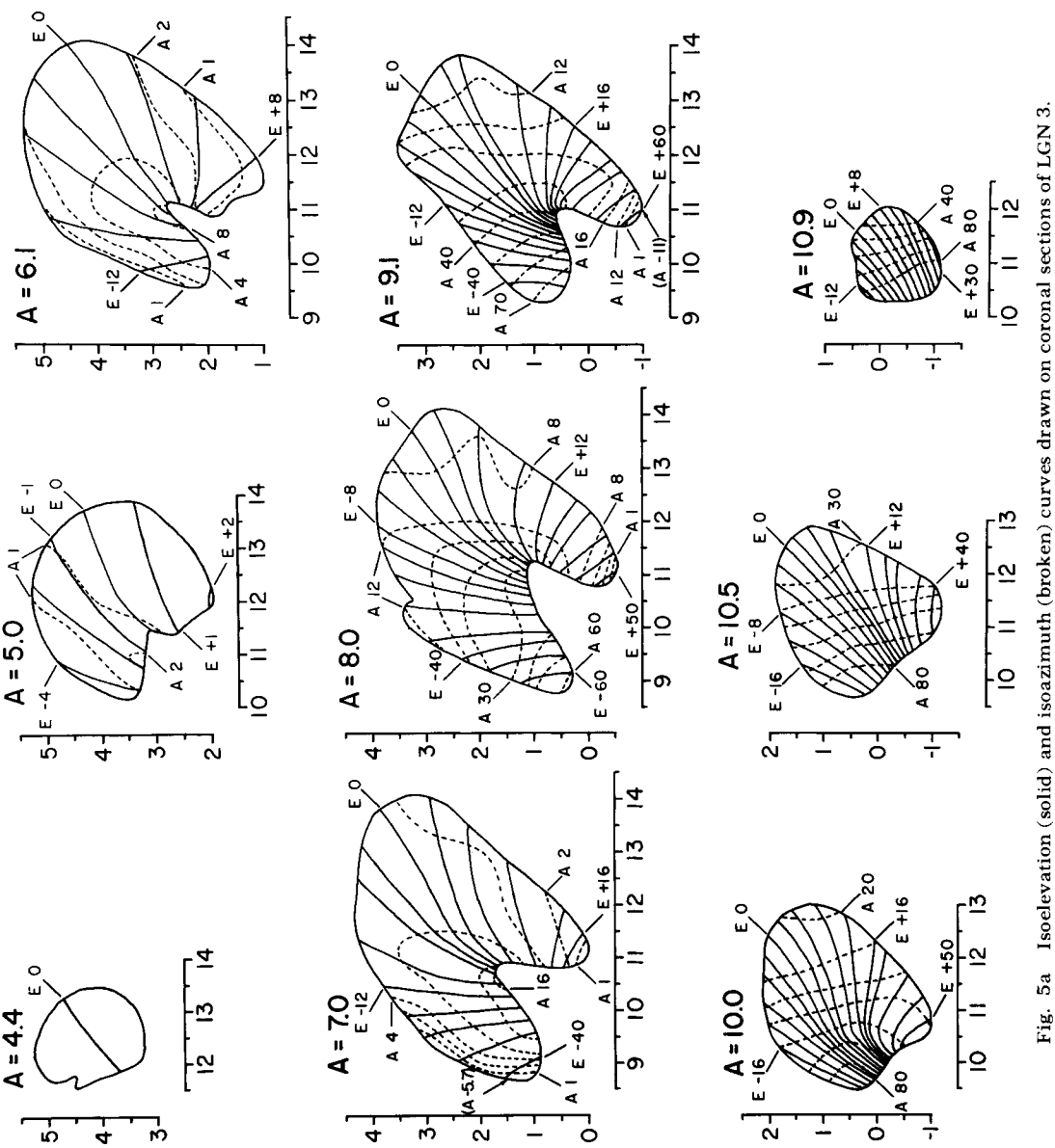

Fig. 5a Isoelevation (solid) and isoazimuth (broken) curves drawn on coronal sections of LGN 3.

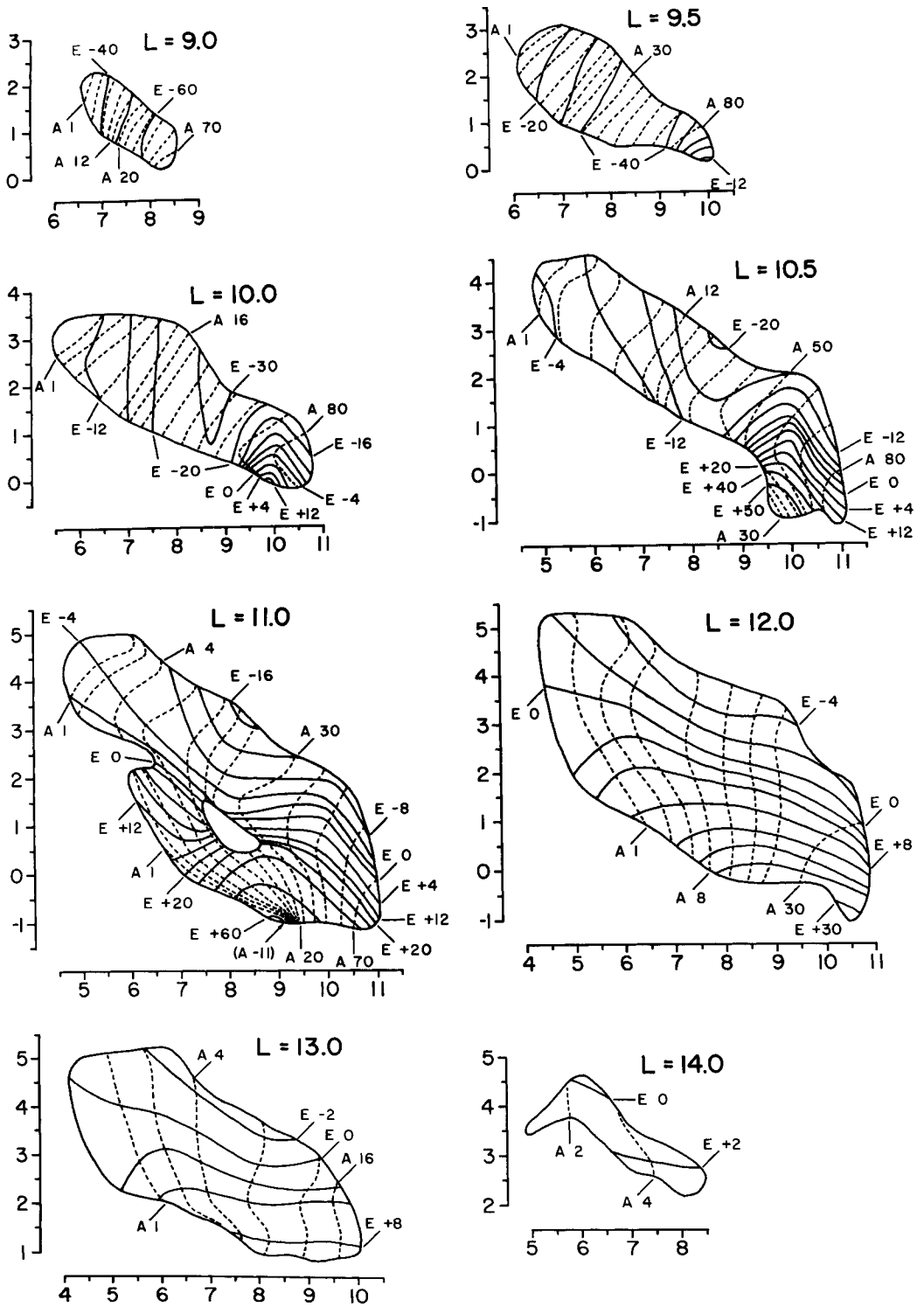

Fig. 5b Isoelevation (solid) and isoazimuth (broken) curves drawn on sagittal sections of LGN 3.

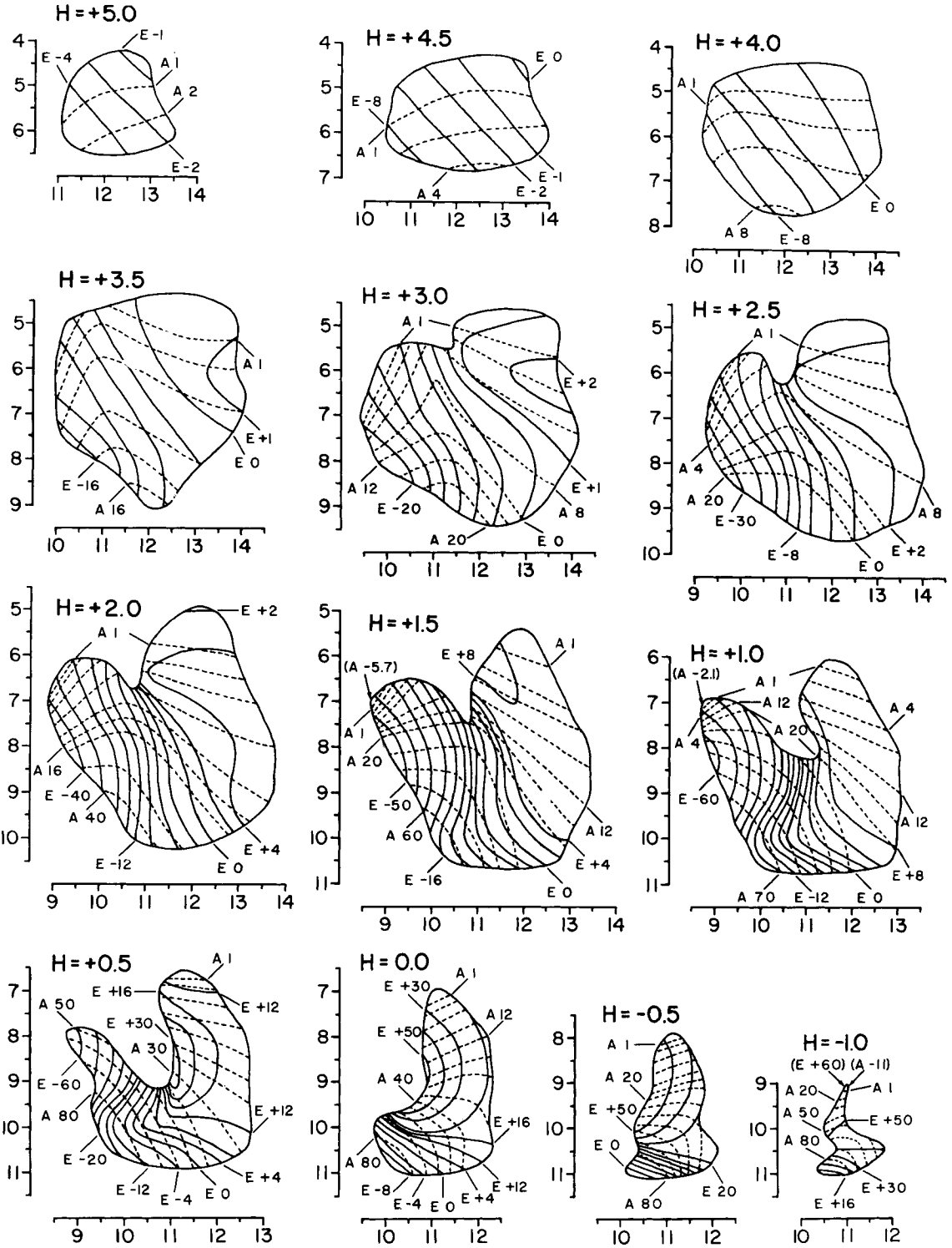

Fig. 5c Isoelevation (solid) and isoazimuth (broken) curves drawn on horizontal sections of LGN 3.

far enough forward on the rim of the lateral wing to reach the very highest elevations, but it does not quite reach the lowest elevations at the tip of the medial wing. Thus, in this monkey at least, the positive vertical meridian is longer than the negative.

The charts presented here allow the determination of paths of projection lines through the LGN. Projection lines fan out from the hylum, passing from the ventral to the dorsal surface. In the central visual fields, the lines are fairly straight and perpendicular to the cell laminae. However, in

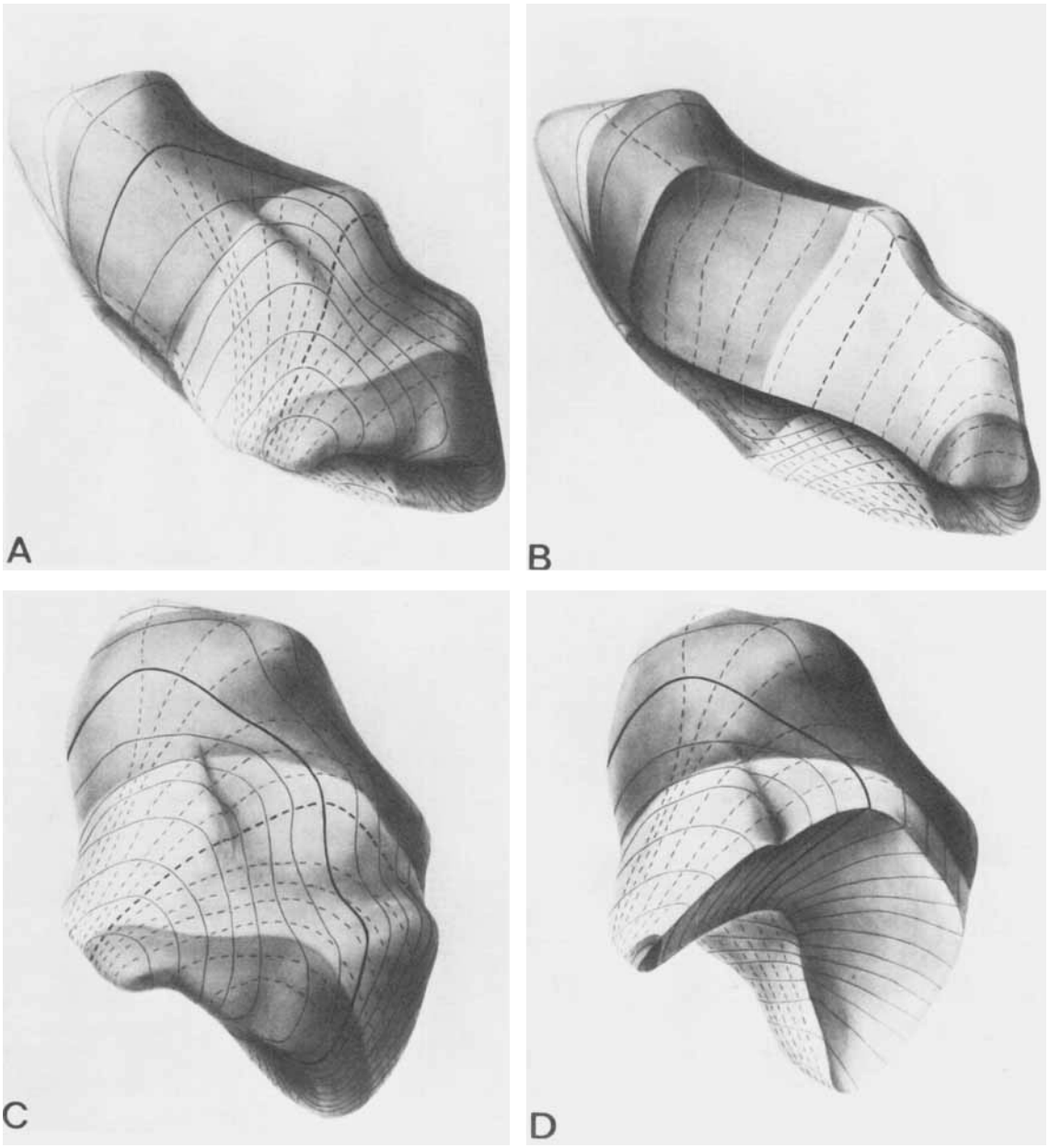

Figure 6

peripheral areas the projection lines generally pass much more obliquely through the laminae. Figures 6b,d show the paths of projection lines along the elevation $-8°$ and the azimuth 20°.

Intersections of isoazimuth and isoelevation planes with the dorsal surface of the dorsal-most cell lamina (layer 6) are shown in a semischematic fashion in figure 8. Here layer 6 is stretched out and unfolded to allow it to lie in a plane. Except for the great expansion of the scale of the central fields, the visual field is mapped onto this surface relatively undistorted. Note that the perimeter of the visual hemifield forms a closed loop around the outer edge of the layer. The vertical meridian is represented by the posterior portion of this loop (heavy broken line) while the outer periphery of the hemifield is represented by the anterior portion (heavy solid line). This cell lamina is not, of course, a two-dimensional structure, but has a certain thickness. Furthermore, several layers are stacked on one another, with visual field locations in register. Thus the hemifield's perimeter is actually represented by a band: the band formed by the exposed edges of the stacked cell laminae. This band is widest posteriorly where there are the most laminae, and narrowest anteriorly where there are the fewest. Visual directions on the perimeter of the visual field are represented by projection lines lying in this band, running, as do all projection lines, from the ventral to the dorsal surface of the LGN. This is also true of the center of the fovea: its projection line, formed by the intersection of the band representing the vertical meridian, and the 0° isoelevation surface, runs vertically along the outer edges of each of the six cell laminae at the posterior pole. The line marked "E 0" in figure 5a (A = 4.4) is just about coincident with the projection line of the center of the fovea.

Two special areas of the LGN, the representations of the fovea and the monocular crescent, are shown in figures 6, 7, and 12. Here we mean *fovea* as defined by Polyak ('57): a circular area of retina of approximately 1 mm diameter, delimited by the rim

Fig. 6 Drawings of solid models of LGN 3 reconstructed from figures 5a,b,c. (a) Medial view with the anterior pole to the right. The standard progression (see the legend of fig. 5) of elevations (solid curves) and azimuths (broken curves) is used. The lowest isoazimuth curve (1°) is to the left while the highest (80°) is to the right. The most negative isoelevation curve ($-60°$) is at the tip of the medial wing (lower foreground). Behind this lies the lateral wing on whose tip may be seen the highest isoelevation curve ($+60°$). The bold solid and broken curves are the $-8°$ isoelevation curve and the 20° isoazimuth curve respectively. Areas delineated by shading, from the posterior pole (upper left) to the anterior pole (lower right), represent: the fovea (light); the rest of the 6-layered binocular field (dark; the 4-layerd binocular field (light); the 2-layered monocular field (dark). (b) Same view as in (a), but all portions of the LGN representing elevations below $-8°$ have been cut away, exposing more of the lateral wing. The cut surface is the $-8°$ isoelevation surface, and its intersections with azimuth surfaces from 1° (left) to 80° (right) are shown. These intersections are projection lines. (c) View of LGN 3 from an anterior-medial aspect. All surface markings are as in (a). (d) Same view as in (c), but all portions of the LGN representing azimuths above 20° have been cut away, exposing the hylum. The cut surface is the 20° isoazimuth surface, and its intersections with elevation surfaces from $-60°$ (left) to $+50°$ (right) are shown. As in (b), these intersections are projection lines.

Drawings by Mrs. Marjorie Greggerman, Medical Art Department, The Johns Hopkins University, School of Medicine.

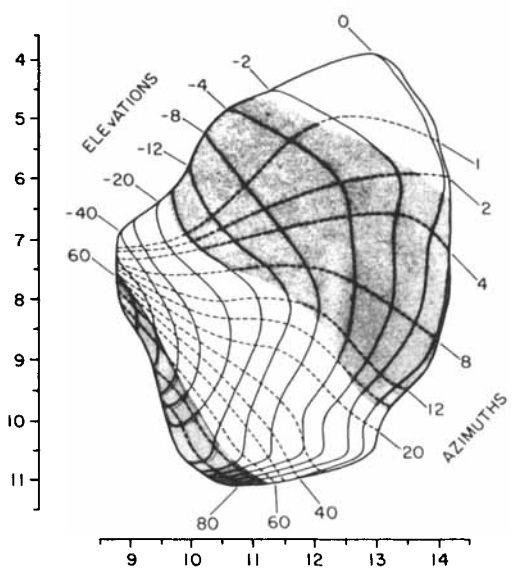

Fig. 7 Projection of the dorsal surface of LGN 3, showing isoelevation (solid) curves and isoazimuth (broken) curves in the standard progression (see the legend of fig. 5). The axes give the Horsley-Clarke anterior (vertical axis) and lateral (horizontal axis) in mm. The shading partitions the LGN into areas representing: the fovea (light); the rest of the 6-layered binocular field (dark); the 4-layered binocular field (light); the 2-layered monocular field (dark).

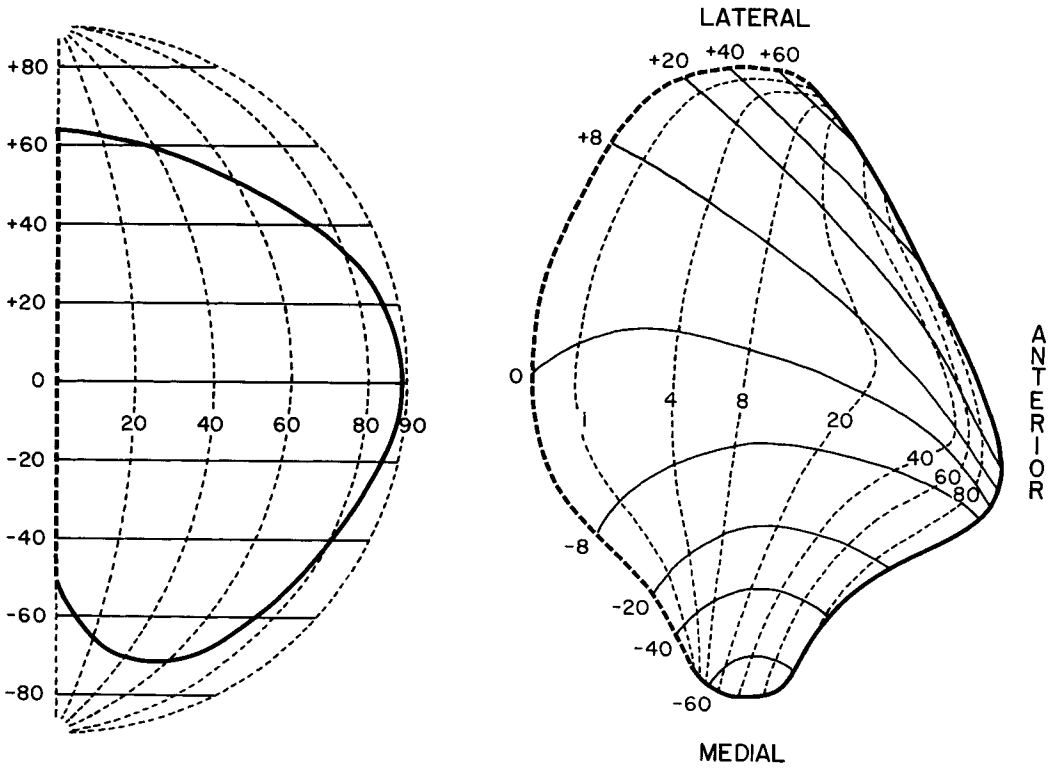

Fig. 8 Semischematic views of monkey 3's right visual hemifield and the projection of this hemifield onto the dorsal surface of layer 6 of her left LGN. Scales are in degrees. The light broken and light solid lines are azimuths and elevations, respectively. The heavy broken and solid lines indicate the perimeter of the hemifield and correspond in both drawings. The surface is of course distorted to lie in a plane. This distortion is primarily in the anterior-posterior direction. Distances within any Horsley-Clarke plane (i.e., medial-lateral distances) are undistorted. Distances along sagittal planes are generally stretched, with the stretching greatest in medial and lateral regions. Anterior-posterior distances along the horizontal meridian are not distorted. Small, local deviations have been smoothed out of the curves.

of the foveal depression. We used a generously large estimate of 5° for the visual angle subtended by this area. Still, the volume of the LGN devoted to the foveal retina is not nearly as large as expected from the results of anatomical studies (Brouwer and Zeeman, '26; Clark and Penman, '34; Polyak, '57). Our estimate of the monocular area of the right visual hemifield of monkey 3 is shown in figure 2. This estimate was obtained by determining the greatest azimuths from which the lateral margin of the ipsilateral pupil could be sighted at various elevations. As we will show in the DISCUSSION, the true monocular area is probably somewhat smaller than indicated (and the binocular area correspondingly larger).

E. *The optic disc projection column*

Bishop et al. ('62) suggested that the cell-free break through layer A in the cat LGN corresponds to the projection column of the optic disc in the contralateral retina. Kass et al. ('73) confirmed this and extended the observation to a variety of species. In monkeys, including *Macaca mulatta*, they found breaks in the most ventral and most dorsal cell laminae. We have also investigated these discontinuities, and present here some additional observations.

The size and position of the optic disc were determined in LGN 3 and one other monkey by using the optical device described in the METHODS section to ascertain the visual field coordinates of its superior, inferior, medial, and lateral margins. In both animals it formed a 7.2° by 5.3° oval, with the long axis vertical, centered at approximately 17° azimuth, 0° elevation. The path of the projection line of the

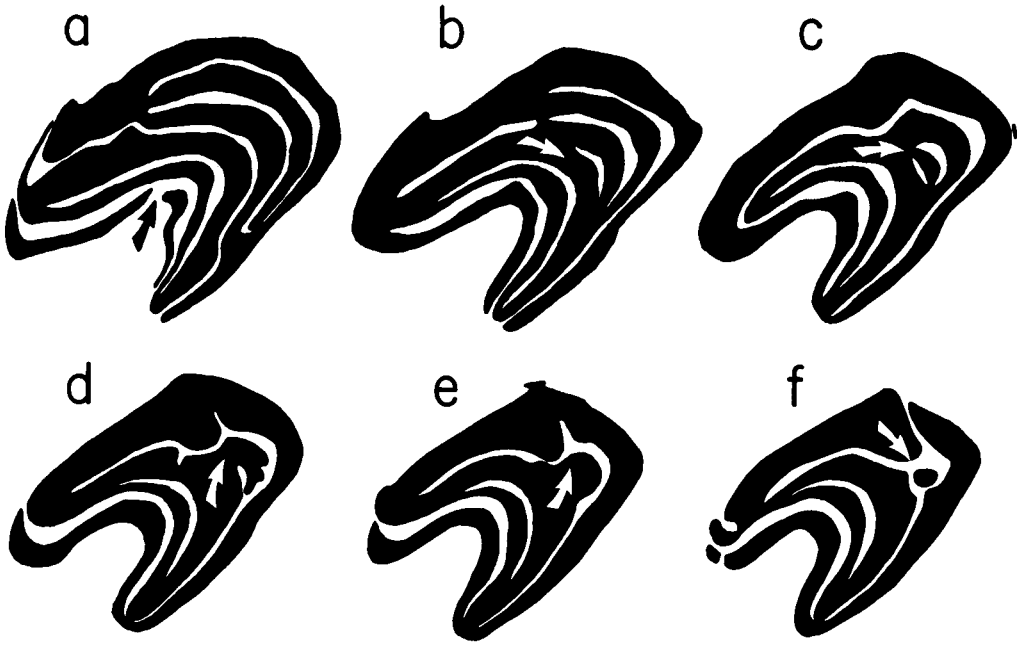

Fig. 9 Tracings of coronal sections of LGN 3 (not corrected for differential shrinkage) showing features of the layering associated with the projection column of the optic disc. The points of the arrows lie on the intersection of the projection line of the center of the optic disc with the coronal plane as determined from figure 5a. From left to right the approximate anterior coordinates of the sections are 7.5, 8.2, 8.6, 8.9, 9.0, and 9.1 mm.

visual direction corresponding to the center of the optic disc was determined from our charts and marked upon tracings of the coronal sections of LGN 3 (fig. 9). We use here the conventional system of numbering layers: 1 to 6, ventral to dorsal. Layers 1, 4, and 6 receive optic tract axons from the contralateral eye whereas layers 2, 3, and 5 are innervated by the ipsilateral eye. Along the route of the optic disc projection line, the following features were observed in this and all other serially sectioned LGN's studied: there is a cell-free break through layer 1 (fig. 9a); layers 2 and 3 appear complete; layer 4 ends, either disappearing at this point or, less commonly, merging with layer 6 (figs. 9c,d); layer 5 also terminates, but before completely disappearing it merges with layer 3, forming a bud or ridge of cells innervated by the ipsilateral eye which extends a variable distance up into a break through layer 6 (figs. 9d,e,f). Although the bud usually protrudes about halfway through layer 6, the break always extends completely through this layer (fig. 9f). Thus the projection line of the center of the optic disc is carried through the nucleus without intersecting layers 1, 4, and 6. The shape and inclination of the layer 6 break as seen in coronal sections are fairly consistent. The break appears as a thin slit oriented inferior-lateral to superior-medial.

These features were also found in an exaggerated form in a LGN from a macaque who had lost one eye, causing the cells of layers 1, 4, and 6 of the contralateral LGN to atrophy (fig. 10). Here, the ipsilateral bud can be seen extending to the surface of the nucleus through a wide break in layer 6.

The projection lines associated with visual directions of retinal points immediately adjacent to the blind spot should enclose a columnar region of the LGN which represents the optic disc of the contralateral retina and the corresponding area of the ipsilateral retina. We have determined from our charts the paths of these projection lines and the portion of LGN 3 which they enclose. Figure 11 shows the intersection of this columnar region with a coronal plane through LGN 3. This is the same coronal section seen in figures 5a (A = 9.1) and 9f. The inclination of this oblong area

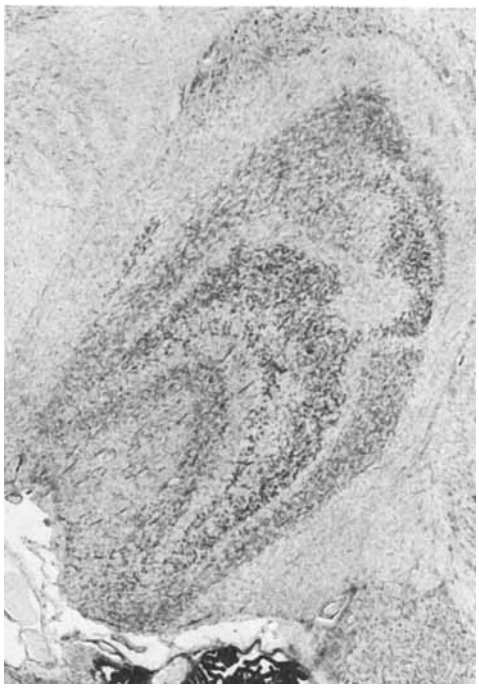

Fig. 10 A coronal section of the LGN of a *Macaca mulatta* whose contralateral eye had been lost an unknown time prior to death. There are four cell layers at this level. The ipsilateral-eye layers stain darker than the contralateral. A plume of cells serving the ipsilateral eye can be seen extending through a break in layer 6 on the right (lateral) side of the section. (From the slide collection of Dr. Gian Poggio, Department of Physiology, The Johns Hopkins University School of Medicine.)

matches the inclination of the layer 6 break, but its width is considerably greater than the slit seen in figure 9f. The width of the oblong area delineated in figure 11 is determined primarily by the adjoining isoazimuth lines. We are confident that they are correctly drawn, since this area was closely bracketed by two penetrations, as indicated in figure 11. The discrepancy has interesting implications, which will be dealt with in the DISCUSSION.

F. *The number of cell laminae devoted to different regions of the visual field*

Anatomical studies have shown that the full complement of 6 cell laminae exists only in the posterior third of the macaque LGN (Clark, '41b; Polyak, '57; Kaas et al., '72). Rostral to this area, there are at most two parvocellular and two magnocellular

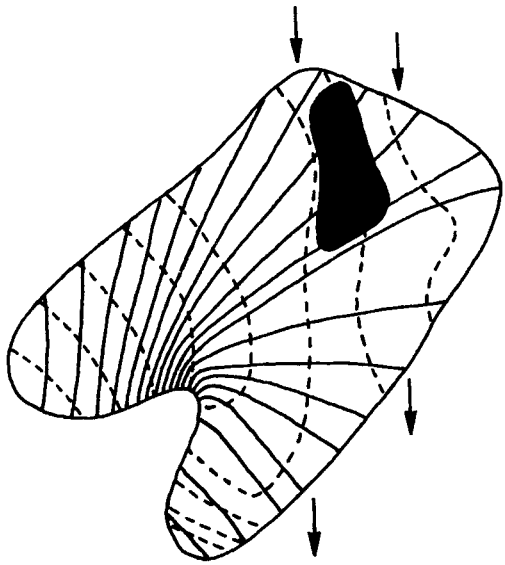

Fig. 11 Coronal section (A = 9.1 mm) from figure 5a on which the region delimited by projection lines corresponding to retina immediately adjacent to the optic disc has been blackened in. The arrows show the paths of the closest microelectrode penetrations at this coronal level.

layers. Since cell layers 4 and 5 end at the optic disc discontinuities, the projection column of the optic disc must lie at the boundary between these regions of the LGN. To determine the complete boundaries of the visual field area represented by 6 cell laminae requires a knowledge of the paths of projection lines. A discrete area of the visual field is represented in a given set of cell laminae if and only if all projection lines representing that visual field area pass through those cell laminae. Determining which layers represent a particular region of visual field is complicated by the fact that projection lines seldom run in Horsley-Clarke planes. Having an accurate idea of the paths of projection lines through LGN 3, along with serial sections of this same LGN, enabled us to make this determination.

Since the four parvocellular layers are reduced to two at the region of the optic disc features, we checked to see whether the reduction of layers takes place at all points the same eccentricity from the foveal center. The region of the LGN representing all points within 17° from the center of the fovea was marked out and found

to coincide well with those regions in which projection lines pass through all six layers. For binocular zones more eccentric than the optic disc, there are four layers: two parvocellular and two magnocellular (layers 1, 2, 3, 6).

We also delineated the portion of the LGN containing the monocular field. Projection lines passing through this area tend to be oriented horizontally. We therefore used the horizontally sectioned companion LGN (right side) of LGN 3 for our comparison. The boundary we have placed between binocular and monocular fields in figure 2 is an estimate only (see Section B of the DISCUSSION). Nevertheless, when this area was marked out on the horizontal series of our visual-field map and compared to the horizontally sectioned nucleus, it was clear that it corresponds well in shape and size to an area of the LGN in which projection lines pass through two layers: a contralateral parvocellular and a contralateral magnocellular layer (layers 1, 6).

The 6, 4, and 2-layered regions of the macaque LGN are delineated in figure 12. The 6-layered region is further divided into foveal and parafoveal areas. These same divisions are indicated in figures 6 and 7 as well.

G. *Nasotemporal overlap*

We saw no evidence of significant nasotemporal overlap in the central visual fields. In the foveal region, the largest negative azimuth found was $-0.4°$. We cannot state our maximum error precisely, but we believe it to be approximately $0.3°$ in the central visual fields for LGN 3. For more extreme elevations, receptive fields further into the ipsilateral hemifield were found (fig. 2). The extremes were $-5.6°$ azimuth at $-37.5°$ elevation and $-11.0°$ azimuth at $+58.0°$ elevation. The actual great circle retinal distances involved are $4.4°$ at $-37.5°$ elevation and $5.8°$ at $+58.0°$ elevation.[3] These are far too large to have resulted from errors in plotting receptive fields or from shifts in the direction of gaze during the course of a penetration. Nor is it likely that eye rotation could account for the results. Both points were found in the same (contralateral) eye, which would have had to rotate approximately $14°$ in the 71-hour interval between the two observations.[4] As explained above in Section C, our data indicate that there was no significant rotational movement of the eyes during the course of the experiment.

H. *Magnification factor*

We define the LGN "magnification factor" as the volume of the nucleus devoted to a unit of solid angle of visual field (dimensions: mm^3/steradian). Assuming that all visual directions equidistant from the center of the fovea have the same magnification, magnification factors can be calculated if one knows the volumes of LGN regions representing different annular areas of visual field. We determined these volumes from the horizontal series of charts (fig. 5c). The visual hemifield from $0°$ to $60°$ (roughly the binocular field) was divided into a series of hemiannuli by lines of constant eccentricity. These eccentricities are listed in the first column of table 1. The areas of an enlarged version of figure 5c representing the delineated annuli were cut out for each horizontal section and weighed. For each annulus, a graph of weight of cut-out area versus position along the Horsley-Clarke vertical was made. The integral of a curve generated by this procedure is proportional to the volume of the nucleus devoted to the corresponding annulus. The absolute volumes, which include interlayer regions, were calculated on the basis of a total volume for LGN 3 of 77 mm^3, and these volumes are listed in a cumulative fashion in column 2. Column 3 gives the solid angle of the visual field corresponding to each of the LGN volumes listed. For these calculations, it was assumed that there is no nasotemporal overlap into the ipsilateral visual hemifield. The derivative of the curve formed by plotting column 2 against column 3 is the magnification factor. These derivatives, at the listed eccentricities, are given in the last column of table 1, and are shown graphically in figure 13.

---

[3] The shortest great circle subtense θ between a visual direction of elevation E, azimuth A and the vertical plane containing the axis of primary visual direction is given by:

$$\theta = \arcsin(\cos E \cdot \sin A)$$

[4] The rotation of the eye about the optic axis, Φ, required to shift a point from the vertical meridian to azimuth A, elevation E is given by:

$$\Phi = \arctan \frac{\sin A}{\tan E}$$

The sum of the two Φ's corresponding to the points of negative azimuth in question equals $14°$.

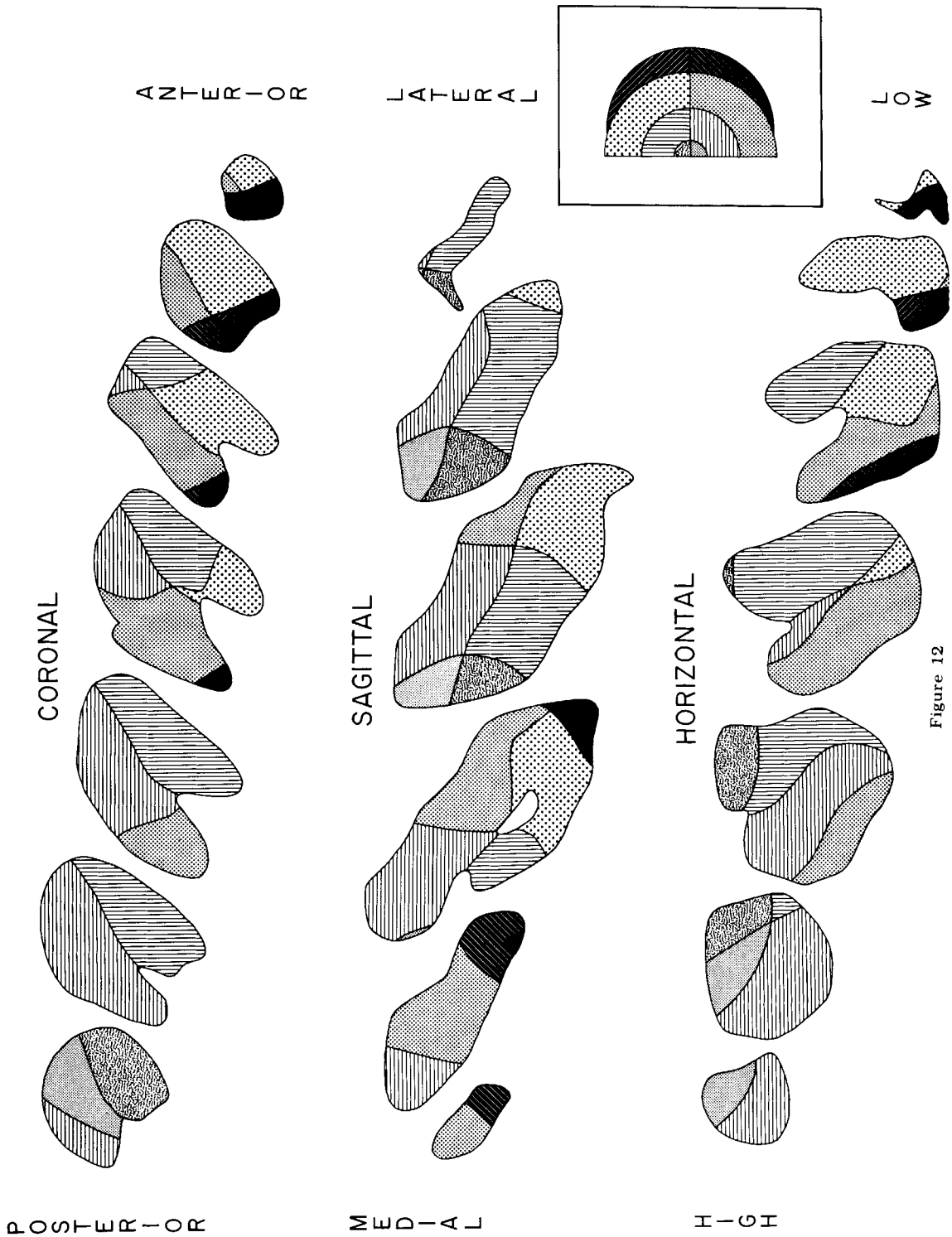
CORONAL
SAGITTAL
HORIZONTAL
POSTER—OR
ANTER—OR
MED—AL
LATERAL
H—GH
LOW

Figure 12

TABLE 1

Eccentricity	LGN volume	Solid angle	Magnification factor
degrees	mm^3	steradians	mm^3/steradian
1	2.2	0.00047	3407
2	6.3	0.00191	2351
4	14.7	0.00766	994
8	27.6	0.03056	422
12	38.5	0.06896	170
16	44.3	0.12206	76
20	49.5	0.18976	59
30	58.1	0.42076	26
40	63.7	0.73496	14
50	68.0	1.12246	8.9
60	71.3	1.57046	5.7
Entire hemifield	77.0	—	—

To compare our calculations of LGN magnification to the retinal magnification data of Rolls and Cowey ('70) and the cortical magnification data of Daniel and Whitteridge ('61), we converted retinal and cortical data into ganglion cells/steradian and mm^2/steradian, respectively. Rolls and Cowey ('70) took cone density as a measure of ganglion cell density within 7° of the center of the fovea, and we used this approximation here. Logarithmic plots of LGN magnification against retinal magnification, and cortical magnification against LGN magnification with eccentricity as a parametric variable are both straight lines with virtually identical slopes (figs. 14, 15).

Our LGN data were not sufficiently detailed to allow us to calculate the LGN magnification at 0°. However, Daniel and Whitteridge ('61) provide these data for the cortex (1.34×10^5 mm^2/steradian), and this may be used to estimate the value of magnification at 0° in the LGN. The line in figure 15 has been extended to intercept the 0° cortical magnification value of the ordinate (triangular symbol), giving an LGN magnification factor of 4715 mm^3/steradian. This is the origin of the 0° LGN magnification shown in figure 13 (triangular symbol). We calculated the retinal magnification factor at 0° from the data in Rolls and Cowey's figure 4 by multiplying the magnification at 5° by the square of the ratio of cone separation at 5° to cone separation at 0°. Again, cone density is used as an approximation of ganglion cell density. This value (1.25×10^7 ganglion cells/steradian), along with the extrapolated value for LGN magnification, determines the coordinates of the 0° point on figure 14 (triangular symbol). The close proximity of this point to the extended line is an indication that linear extrapolations [on a logarithmic scale] to 0° eccentricity are valid. The extrapolated value of retinal magnification at the center of the fovea is 1.41×10^7 ganglion cells/steradian.

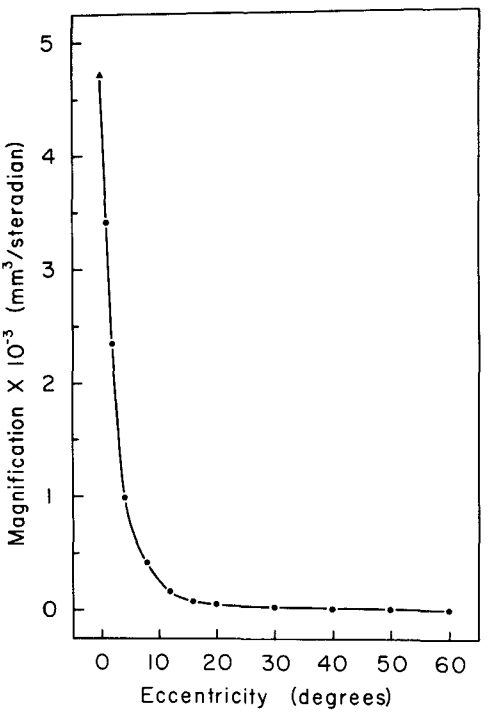

Fig. 13 LGN magnification factor as a function of visual field eccentricity. The 0° eccentricity value (triangle) is derived from figure 15.

Fig. 12 Coronal (top), sagittal (middle), and horizontal (bottom) series showing the portions of the LGN representing various areas of the visual field. Orientations are the same as in figures 5a,b,c. The insert at the right of the figure shows schematically the areas dealt with: the fovea (2.5° radius, 6 cell layers); the rest of the central visual field out to the optic disc (17° radius, 6 cell layers); the remainder of the binocular field (4 cell layers); the monocular crescent (2 cell layers). Each of these zones is further divided into upper and lower visual fields. The vertical axes of both the coronal and sagittal sections, and the anterior axes of the horizontal sections, are aligned across the figure. Levels shown (from left to right) are: coronal A = 5.0, 6.1, 7.0, 8.0, 9.1, 10.0, and 10.9 mm; sagittal L = 9, 10, 11, 12, 13, and 14 mm; horizontal H = +5, +4, +3, +2, +1, 0, and −1.

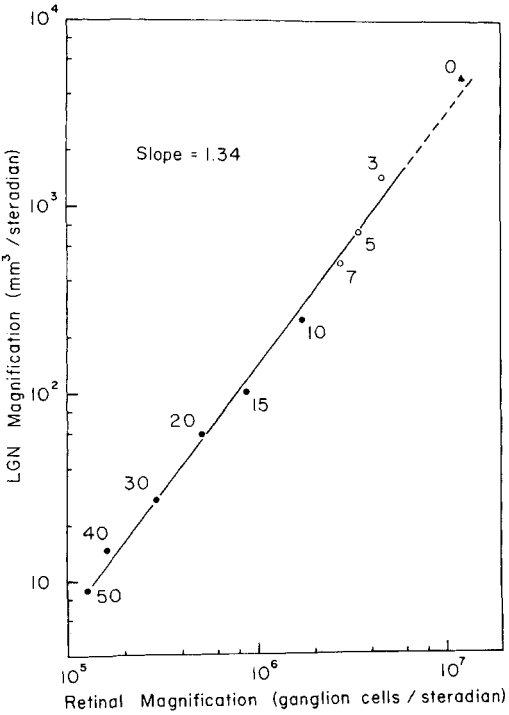

Fig. 14 LGN magnification as a function of retinal magnification (linear regression: correlation coefficient = 0.997). The labeled graphical symbols refer to eccentricities. Filled circles are derived from ganglion cell densities while unfilled circles are derived from cone densities, used here as approximations of ganglion cell densities (Rolls and Cowey, '70). The source of the 0° eccentricity point (triangle) is explained in the text.

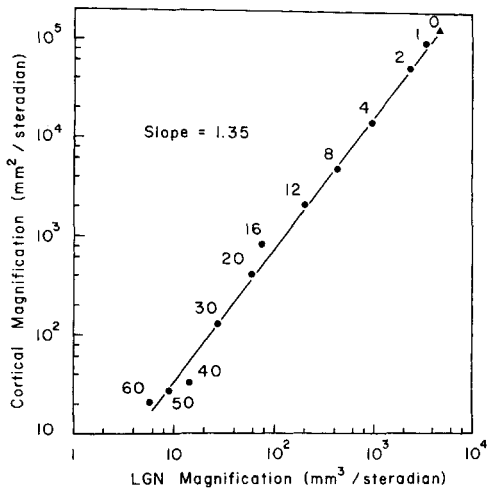

Fig. 15 Cortical magnification as a function of LGN magnification (linear regression: correlation coefficient = 0.997). The labeled graphical symbols refer to eccentricities. The LGN magnification factor at 0° eccentricity is determined by extrapolating the fitted line to the 0° cortical magnification (triangle). Cortical values are from Daniel and Whitteridge ('61).

For that portion of the visual field dealt with in our experiments, the range of LGN magnifications is approximately three decades. Clearly, since the slopes of the lines in figures 14 and 15 are larger than 1, the representation of the central visual fields relative to peripheral fields increases greatly at each step along the primary visual pathway from retina to striate cortex. These relationships may be expressed by the following equations derived from figures 14 and 15:

$$\frac{M_{lgn}(e_1)}{M_{lgn}(e_2)} = \left[\frac{M_{ret}(e_1)}{M_{ret}(e_2)}\right]^{1.34}$$

$$\frac{M_{cor}(e_1)}{M_{cor}(e_2)} = \left[\frac{M_{lgn}(e_1)}{M_{lgn}(e_2)}\right]^{1.35}$$

$$\frac{M_{cor}(e_1)}{M_{cor}(e_2)} = \left[\frac{M_{ret}(e_1)}{M_{ret}(e_2)}\right]^{1.34\times1.35} = \left[\frac{M_{ret}(e_1)}{M_{ret}(e_2)}\right]^{1.81}$$

where $M_{lgn}(e)$, $M_{ret}(e)$, and $M_{cor}(e)$ are the magnifications of the LGN, retina, and striate cortex, respectively, at angular eccentricity e.

As an example, the ratio of magnification at 0° eccentricity to magnification at 50° for the retina is approximately 108 ($1.41 \times 10^7 \div 1.31 \times 10^5$), while the ratios for the LGN and cortex at these eccentricities are 530 ($108^{1.34}$) and 4760 ($108^{1.81}$) for the LGN and cortex, respectively.

DISCUSSION

A. *Comparison of the results of anatomical and electrophysiological mappings*

Previous investigations of the functional topography of the monkey LGN have either been presented in the polar coordinate system of visual field perimetry (Kaas et al., '72; Whitteridge, '73) or can best be understood in these terms (Brouwer and Zeeman, '26; Polyak, '57). In this system, a visual direction is located by its angular eccentricity from the fixation point, and the inclination of the meridian on which it lies with respect to the horizontal meridian.[5]

[5] Eccentricity (e) and inclination (i) convert to azimuth (A) and elevation (E) by the formulae: A = arc tan(tan e · cos i); E = arc tan(sin e · sin i).

The annular area between two lines of constant eccentricity is known as a "zone." Although our charts are drawn in terms of azimuths and elevations, the LGN regions delineated by shading in figures 6, 7, and 12 show the representations of three zones (and the monocular crescent), and serve as a convenient basis for comparing our results with those of other workers.

The generally held view of the topographic representation of the visual field in the macaque LGN has been based primarily upon the experiments of Brouwer and Zeeman ('26) and Polyak ('57), who used Marchi techniques to trace the paths of degenerating axons into the nucleus after placing lesions in the retina. Their conclusions were similar and substantially correct. However, the extent of the foveal projection was greatly overestimated, imposing a considerable distortion on the overall topography of the visual field representation. In their summary diagrams (Brouwer and Zeeman, '26, fig. 23; Polyak, '57; fig. 225), the upper and lower macular quadrants form wedges on either side of the LGN's plane of symmetry. Although largest posteriorly, the macular segment extends all the way to the anterior pole. Upper and lower portions of zones project symmetrically to either side of this central segment, with the most peripheral zones represented in the tips of the medial and lateral wings of the nucleus. Thus, in their view, the central zones intrude between upper and lower peripheral fields. The flanking segments are connected only by thin bridges running over the anterior portion of the hylum. Polyak ('57) believed that for the most-peripheral fields the division is complete and the mapping is not topographically continuous across the peripheral horizontal meridian.

Figures 6, 7, and 12 show that the projection is organized according to somewhat different principles. Zones simply project serially along the major axis of the nucleus. There is no intrusion of central visual fields between peripheral upper and lower fields. The fovea is strictly limited to the posterior pole, accounting for at most 12% of the total volume of the LGN. The mapping is completely continuous across the horizontal meridian, even in the monocular area.

Results of electrophysiological mappings done in other laboratories are compatible with our views. Kaas et al., ('72) showed that, in the owl monkey, central visual fields are restricted to the posterior pole. They also described the placement of the vertical meridian and the monocular crescent. In addition, Whitteridge ('73) has published a semischematic map (in polar coordinates) of the dorsal surface of layer 6 which is in close agreement with our results.

Given the basic limitations of the anatomical methods employed in the early mappings, it is not surprising that the topography was distorted to some extent. The difficulty of producing discrete retinal lesions was compounded by the interruption of retinal ganglion cell axons passing through the lesioned area. Furthermore, the Marchi method does not allow one to readily distinguish fibers of passage from terminating fibers. Another factor which contributed to this distortion was the assumption of complete visual-field symmetry about the morphological plane of symmetry of the LGN. All of the lesions which Polyak ('57) traced into the LGN were made above the retina's horizontal meridian. Upper peripheral retina projects to the medial wing of the nucleus, and he assigned lower peripheral retina to the corresponding point in the tip of the lateral wing, further exaggerating the separation of upper and lower fields. Figure 12 shows that the lower peripheral retina (upper visual field) actually projects to the anterior pole.

The problems inherent in the Marchi method were avoided by Clark and Penman ('34) who used transneuronal degeneration to assess the effects of retinal lesions. Unfortunately, while they recognized that the foveal representation is much less extensive than had been suggested by Brouwer and Zeeman, they still thought that it extends as a narrow median sector fairly far anteriorly. We believe that their foveal lesions must have involved fibers which originate along the temporal horizontal meridian and skirt the foveal depression on their way to the optic disc. Thus they did not fully counter Brouwer and Zeeman's ('26) notion of a macular segment interposed between upper and lower visual fields, an idea later reinforced by Polyak's ('57) conclusions.

One final potential source of confusion results from the orientation of the LGN with respect to Horsley-Clarke planes. Roughly speaking, semicircles of equal eccentricity project onto planes in the LGN

which are perpendicular to its main axis. If, however, the nucleus is cut in a plane oblique to these surfaces of equal eccentricity, zones over a range of eccentricities will be represented in a single section. Because of this, the simple zonal structure of the visual field representation in the LGN will not be revealed by experiments in which only a few points are mapped and only one plane of section considered. An example of this may be seen in figure 12, which gives the impression that peripheral zones in the wings flank central zones in the main body of the LGN. Likewise in figure 3, the 6-layered central region seems to be interposed between 4-layered regions in the wings of the nucleus. Figure 6a and the sagittal sections in figure 12 make it clear that this is an illusion. Because of the forward tilt of the nucleus, ventral and dorsal areas of a coronal section do not correspond to the same anterior-posterior level relative to the main axis of the nucleus. For sections cut in the appropriate plane, the medial and lateral wings would represent approximately the same zone as the main body of the LGN.

This brief review demonstrates that there can be serious difficulties in the interpretation of experiments designed to elucidate the topographical representation of visual fields using anatomical methods alone. Even though the workers who employed these techniques were fully aware of the pitfalls inherent in them, they were still misled on several important points. Electrophysiological mapping techniques avoid all these problems.

Postmortem evaluation of the effects of retinal lesions in human LGN's is subject to the same difficulties. Kupfer ('62) has reported that the fovea of the human is represented as far anteriorly as two-thirds to three-fourths of the length of the LGN from the posterior pole. His view is based on the extent of cell atrophy in the nucleus resulting from macular lesions. It would be surprising if the scale of representation of the central visual fields in the human LGN differs so drastically from that of the monkey. Kaas et al. ('73) have demonstrated that the features associated with the optic-disc projection column are found in a wide variety of species. Perhaps they can be recognized in the human LGN and used to place definitive limits on the extent of the central retinal projection.

B. *Features of the cell lamination*

With respect to the number of cell layers, our data show that there are three distinct portions of the LGN in which projection lines pass through 6, 4, or 2 cell laminae. The transitions between these three regions of the nucleus are well defined. Both retinal (Rolls and Cowey, '70) and LGN magnification factors increase dramatically in the central visual field. Whether the doubling of parvocellular layers is an accommodation to these accelerating magnification factors, or whether it marks some functional transition, is an unresolved question.

Given that peripheral binocular visual fields are represented by two contralateral and two ipsilateral layers, one would predict that the monocular crescent area would consist of no more than two layers. The fact that it is represented by two layers means that all parts of the visual field project to both magnocellular and parvocellular laminae. This is in agreement with Kaas et al. ('72) scheme of the basic organization of the primate LGN. The location of the monocular crescent area at the inferior-medial part of the anterior pole results in its receiving the brunt of the incoming optic tract fibers. In horizontal sections, large bundles of axons can be seen coursing through the monocular area. This portion of the LGN seems much more broken-up by optic-tract fiber bundles than any other. Most of the binocular area of the LGN is spared this disruption.

The area of visual field which is monocular (fig. 2) is an estimate only. With the eyes directed forward, the visual field of each eye is partially blocked by the nose and other features. The area of binocular overlap is larger and the monocular field smaller when the eyes are deviated to one side. It is the absolute monocular area which presumably corresponds to the portion of the LGN consisting of only two layers. The method we used to estimate the extent of the monocular crescent measures the functional monocular crescent in the forward-looking position, thus tending to overestimate the size of the absolute monocular crescent. However, the scale of representation is such that moderate changes

in the estimate of the boundaries of the monocular and binocular areas of vision lead to minor changes in the size, shape, and location of the monocular representation in the LGN.

The most-peripheral visual direction, close to the horizontal meridian, which we recorded was at an azimuth of 83°. We have not drawn azimuth curves beyond 80° in any of our figures, but a conservative extrapolation indicates that fields at least as far out as 90° were represented in LGN 3.

We have confirmed the observations of Kaas et al. ('73) on the existence of breaks in layer 1 and layer 6 corresponding to the optic disc in *Macaca mulatta*. In addition, we find that the termination of layer 4 at this point, combined with the fusion of the remnant of layer 5 with layer 3, results in the projection column of the optic disc being carried upward part-way into the layer 6 break by cells associated with the ipsilateral eye. This should not be considered a disruption of the overall pattern of the ipsilateral layers, since the ipsilateral-eye protrusion is not formed so much by a welling up of cells, as it is by what remains after most of layer 5 and all of layer 4 have terminated.

In all LGN's which we have studied in serial coronal section (except for the abnormal LGN in fig. 10), the size, shape, and inclination of the layer 6 break (fig. 9f) have been quite similar. Bishop et al. ('62) suggest that such a break would avoid distortion of the pattern of nearby projection lines. Kaas et al. ('73) point out that projection lines should run parallel to the columnar breaks. Why, then, does the break seen in figure 9f appear to pass at right angles to the direction of projection lines? The reason is simply that projection lines generally do not run in Horsley-Clarke planes. What one sees in this coronal section results from (although, as we point out below, is not identical to) the intersection of a projection column with the section. The shape of the break is determined by the inclination of the projection column with respect to the coronal plane and by the shape of the column. Clearly, one should be quite cautious about judging the paths of projection lines adjacent to such gaps in other species on the basis of histological sections alone.

We have examined (RESULTS, Sect. E) the columnar region in layer 6 delimited by projection lines corresponding to retinal points adjacent to the optic disc. Our reconstruction indicates that this region is much larger than the cell-free break associated with the blind spot. We conclude that the scale of representation in layer 6 immediately adjacent to the optic disc break must be greatly expanded.

The work of Kalil ('72) suggests a mechanism to account for this expansion. He found that if one eye of a newborn kitten is removed, optic tract fibers from the other eye invade the deprived layer A of the contralateral LGN. The optic disc region of layer 6 is potentially a small region of deprived neurons. We hypothesize that optic tract fibers initially innervate the embryonic LGN in a strict topological mapping, leaving a column of cells in layer 6 corresponding to the optic disc. Sprouts from adjacent axon endings then invade the column to make contact with cells around its periphery, thus reducing the final size of the uninnervated region and changing the scale of magnification. The final size of the optic disc discontinuity may be determined by factors which prevent the innervation of adjacent cells by axon endings originating from separated regions of retina.

We cannot provide evidence that this same process results in the layer 1 break. Here the overall scale of representation is much compressed, and we cannot resolve changes in the scale adjacent to the break. Furthermore, the optic-disc projection column is much narrower in the ventral LGN, and the layer 1 break is large enough to account for it. However, this may only be coincidental. The layer 1 break is the same width as the layer 6 break and may very well represent a minimal distance which is maintained between LGN cells with input from nonadjacent retinal ganglion cells. Similar narrow cell-free regions are found between disparate areas of the abnormal layer A 1 of the Siamese cat (Guillery, '69).

Kaas et al. ('73) have raised the question of whether the optic disc gaps are due to interlaminar mechanisms (i.e., precise registry of homonymous retinal points in adjacent laminae) or are the results of intralaminar mechanisms. For the layer 6 break of *Macaca mulatta*, our hypothesis provides

an answer: although adjacent layers generally are precisely aligned, the break observed is due to an intralaminar mechanism.

Our view of the origin and nature of the optic disc breaks leads to questions as to the representation of the optic disc in the cerebral cortex. It seems reasonable to expect that the pattern of projection from ipsilateral-eye layers of the LGN to striate visual cortex is undisturbed by the optic disc. How are LGN fibers from the contralateral laminae adjacent to the optic disc discontinuities laid down upon this topographically normal pattern? Do they project to homonymous points in a narrow ring around a contralateral-eye deprived area? Or, perhaps, do the "extra" LGN cells project into the cortical optic disc area, giving rise to a region of cortex in which the neurons have abnormally disparate receptive fields?

C. *Magnification factor*

In comparing magnification factors of different structures in the primary visual pathway, appropriate dimensions must be chosen. We decided to use measures of the proportion of the neural apparatus devoted to a unit area of visual field. For the LGN, cells/steradian would have been the logical choice. The microelectrode penetrations made through LGN 3 enabled us to compensate for differential shrinkage during histological preparation and to reconstruct its overall size and shape accurately. However, we could not do this for individual cell laminae with enough precision to allow us to make cell density measurements which would be meaningful for this purpose. Therefore we have used volume/steradian for the LGN magnification factor, along with ganglion cells/steradian for the retina, and cortical area/steradian for the cortex.

Based on volume calculations, the LGN appears to be an intermediate step in the magnification changes which take place between retina and striate cortex. However, the range of the LGN magnification factor derived from cell counts would undoubtedly be greater than the three decades derived from nucleus volume, since the parvocellular-layer cell-density for anterior LGN is less than for the posterior portion of the nucleus (Clark, '41b). Also, the magnocellular layers, which have a relatively low cell density, make up more of the nucleus in its anterior regions than in its posterior regions. Thus the differences between retinal and LGN magnification are probably understated by our data, while differences between LGN and cortical magnification are overstated. Would a LGN magnification function based on cell counts, rather than nucleus volume match the cortical magnification function (i.e., would the slope of fig. 15 be 1)? This, we believe, is unlikely. Figure 16 shows the ratio of cortical magnification to LGN magnification plotted as a function of eccentricity. This ratio for the center of the fovea is approximately 10 times that for the peripheral fields. The cell density at the posterior pole would have to be 10 times that at the anterior pole to extend the range of LGN magnification to match that of the cortex. Clark ('41b) reported the LGN cell density to vary by a factor of approximately 2 in this direction, but since he did not consider the possibility of differential shrinkage we hesitate to use these data quantitatively. However, even though the exact extent of cell density nonuniformity is not known, we judge a variation of a factor of 10 to be improbable.

If our conclusions about the relationship of the LGN to the overall change in magnification between retina and cortex are correct, the distribution of optic radiation fibers

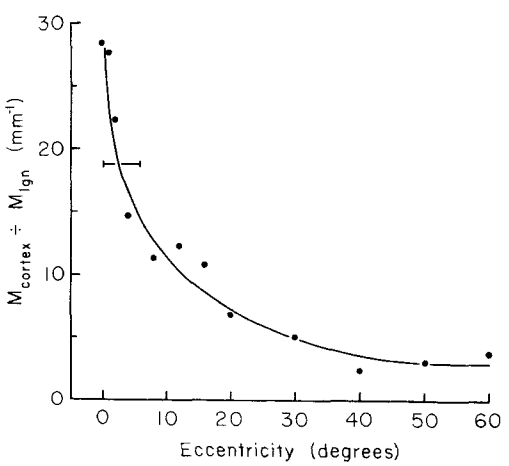

Fig. 16 Ratio of cortical magnification (M_{cortex}) to LGN magnification (M_{lgn}) as a function of eccentricity. Cortical values are from Daniel and Whitteridge ('61) and retinal values are from table 1. The horizontal bracket is discussed in the text (Sect. C of DISCUSSION).

to the striate cortex is uneven. Barring compensatory bifurcation of axons of relay cells of the posterior LGN, the cortical area representing central visual fields must receive a lower density of radiation fibers than peripheral areas. The mode of distribution of optic radiation fibers was investigated by Clark ('41b), who came to different conclusions. He lesioned a small area of the striate cortex and counted LGN neurons in the affected region of the LGN and in the entire nucleus. Since the ratio of the area of the lesion to the number of atrophied LGN neurons was approximately the same as the ratio of total area of striate cortex to total number of LGN neurons, he suggested that the distribution of optic radiation fibers to the cortex is uniform. However, there is an explanation for this apparent conflict between our data and Clark's. The ratio of total area of the striate cortex of one hemisphere (1445 mm^2 as measured by Clark, '41b) to the total volume of LGN 3 (77 mm^3) is 18.8 mm^{-1}. This ratio is obtained at a visual field eccentricity of 2° to 3°, as shown by the intersection of the horizontal bracket with the curve in figure 16. Clark's results can be reconciled with ours by assuming that the lesioned cortical area, which was "immediately behind the sulcus lunatus," happened to correspond to this eccentricity. This is quite possible, since the center of this exposed strip of postlunate cortex represents an eccentricity of approximately 3° (Talbot and Marshall, '41). The entire range of eccentricities covered by this area is only 0° to 6° (the horizontal extent of the bracket in figure 16).

We have no functional interpretation of the mathematical expressions relating magnifications at the different neural levels. Because of the differences which would probably result from using cell counts instead of volume for such calculations, it would be unwise to attach any great significance to the equality of slopes of the two power functions. In our view, the important observation is that the LGN accounts for a large portion of the change in central magnification relative to peripheral magnification which occurs between retina and visual cortex. The participation of the LGN in this great expansion of neural apparatus devoted to central fields may be an important function of the nucleus in the processing of visual information along the primary visual pathway.

ACKNOWLEDGMENTS

We thank Dr. Gian Poggio for his suggestions on the manuscript and Mrs. Dolores Taylor for her technical assistance.

This research was supported by National Institutes of Health Research grant 5 R01 EY00927 and by National Institutes of Health Training grant in Physiology 5 T01 GM00443.

LITERATURE CITED

Bishop, P. O., W. Burke and R. Davis 1962 The identification of single units in central visual pathways. J. Physiol., *162*: 409–431.

Bishop, P. O., W. Kozak, W. R. Levick and G. J. Vakkur 1962 The determination of the projection of the visual field onto the lateral geniculate nucleus in the cat. J. Physiol., *163*: 503–539.

Bishop, P. W., W. Kozak and G. J. Vakkur 1962 Some quantitative aspects of the cat's eye: axis and plane of reference, visual field coordinates and optics. J. Physiol., *163*: 466–502.

Brouwer, B., and W. P. C. Zeeman 1926 The projection of the retina in the primary optic neuron in monkeys. Brain, *49*: 1–35.

Clark, W. E. L. 1941a Observations on the association fibre system of the visual cortex and the central representation of the retina. J. Anat., *75*: 225–235.

——— 1941b The laminar organization and cell content of the lateral geniculate body in the monkey. J. Anat., *75*: 419–433.

Clark, W. E. L., and G. G. Penman 1934 The projection of the retina in the lateral geniculate body. Proc. Roy. Soc. B, *114*: 291–313.

Daniel, P. M., and D. Whitteridge 1961 The representation of the visual field on the cerebral cortex in monkeys. J. Physiol., *159*: 203–221.

Guillery, R. W. 1969 An abnormal retinogeniculate projection in Siamese cats. Brain Res., *14*: 739–741.

Kaas, J. H., R. W. Guillery and J. M. Allman 1972 Some principles of organization in the dorsal lateral geniculate nucleus. Brain Behav. Evol., *6*: 253–299.

——— 1973 Discontinuities in the dorsal lateral geniculate nucleus corresponding to the optic disc: A comparative study. J. Comp. Neur., *147*: 163–180.

Kalil, R. E. 1972 Formation of new retino-geniculate connections in kittens after removal of one eye. Anat. Rec., *172*: 339–340.

Kupfer, C. 1962 The projection of the macula in the lateral geniculate nucleus of man. Amer. J. Ophthal., *54*: 597–609.

Poggio, G. F., F. H. Baker, Y. Lamarre and E. R. Sanseverino 1969 Afferent inhibition at input to visual cortex of the cat. J. Neurophysiol., *32*: 892–915.

Polyak, S. 1957 The Vertebrate Visual System. University of Chicago Press, Chicago, pp. 288–389.

Rolls, E. T., and A. Cowey 1970 Topography of

the retina and striate cortex and its relationship to visual acuity in rhesus monkeys and squirrel monkeys. Exp. Brain Res., *10*: 298–310.

Sanderson, K. J. 1971 The projection of the visual field to the lateral geniculate and medial interlaminar nuclei in the cat. J. Comp. Neur., *143*: 101–117.

Talbot, S. A., and W. H. Marshall 1941 Physiological studies on neural mechanisms of visual localization and discrimination. Amer. J. Ophthal., *24*: 1255–1264.

Whitteridge, D. 1973 Projection of optic pathways to the visual cortex. In: Handbook of Sensory Physiology. Volume VII/3. R. Jung, ed. Springer-Verlag, Berlin and Heidelberg, pp. 249–250.